Chinese Chemical Letters 35 (2024) 108445

Contents lists available at ScienceDirect

Chinese Chemical Letters

journal homepage: www.elsevier.com/locate/cclet

Ultrathin ternary PtNiGa nanowires for enhanced oxygen reduction reaction

Giday Fisseha[a], Yiping Hu[a,*], Yanan Yu[a], Shaojie Lu[a], Dongsheng Ma[a], Pei Nian[b], Zheng Wang[b], Qin Yue[a,*]

[a] Institute of Fundamental and Frontier Sciences, University of Electronic Science and Technology of China, Chengdu 610054, China
[b] State Key Laboratory of High-efficiency Utilization of Coal and Green Chemical Engineering, School of Chemistry and Chemical Engineering, Ningxia University, Yinchuan 750021, China

ARTICLE INFO

Article history:
Received 19 January 2023
Revised 11 March 2023
Accepted 12 April 2023
Available online 13 April 2023

Keywords:
Ultrathin nanowires
Gallium
Oxygen reduction reaction
Ternary alloy
Durability

ABSTRACT

Achieving high activity and durability for the oxygen reduction reaction (ORR) with an ultra-low amount of platinum is significant to promote the widespread application of proton exchange membrane fuel cells (PEMFCs). Here we report a new ultrathin (~1 nm) ternary PtNiGa alloy nanowires (PtNiGa NWs) electrocatalyst, in which the presence of gallium (Ga) enhances the oxidation resistance of platinum (Pt) and nickel (Ni) and suppresses the dissolution of Ni. The mass and specific activities of PtNiGa NWs are about 11.2 and 7.6 times higher than those of commercial Pt/C catalysts for ORR. Moreover, the mass activity of PtNiGa/C NWs nanocatalyst decreased only by 12.8% and largely retained its electrochemical surface area (ECSA) after 10,000 potential cycles, compared with 38% loss of ECSA for commercial Pt/C catalyst. Therefore, this work provides a general guideline for preparing ternary alloy electrocatalysts and enhancing the activity and stability of the cathode ORR reaction of PEMFCs.

With the growing concern over the increasing depletion of conventional fossil fuels, the search for renewable and environmentally friendly energy solutions is urgent [1]. Proton exchange membrane fuel cells (PEMFCs) are considered as the most promising energy conversion devices for zero-emission, sustainable and high energy conversion efficiency [2–5]. However, the sluggish oxygen reduction reaction (ORR) at the cathode is one of the key limitations for the widespread applications of PEMFCs [6–8]. Pt-based nanocrystals are considered as the most efficient and favorable electrocatalysts for cathodic oxygen reduction reactions [9–12]. However, the high cost and low utilization efficiency associated with Pt-based electrocatalysts largely hinder their widespread applications in ORR [13–15]. Hence, one of the most significant approaches to enhance Pt mass activity and utilization efficiency towards ORR is alloying of Pt with 3d transition metals (Fe, Ni, Co, Cu, *etc.*) [16], which help lowering the center of the d-band, optimizing the adsorption conditions for intermediates (*e.g.*, OH_{ads}) and tuning the surface composition by exposing specific facets employing ligand or optimized geometric factors [17–21]. Stamenkovic *et al.* demonstrated that binary annealed Pt_3Ni is active with its well-defined (111) facets and its synergistic effect reveals superior ORR activity than that of the commercial Pt/C catalysts [22].

However, the limited long-term durability caused by the gradual leaching of 3d transition metals, as well as decreased ECSA because of irreversible agglomeration of the alloy nanoparticles (NPs) under corrosive conditions appears to be the major challenges of binary Pt-based alloy (PtM) nanocrystals in practical ORR applications. Some distinctive approaches are achieved to inhibit the dissolution of transition metals in alloy. On the one hand, by geometric morphology control methods (*e.g.*, one-dimensional (1D) nanowires (NWs), nanotubes) [11,23–28], and on the other hand, by incorporating PtM with a third transition metal (*e.g.*, Fe, Mo and Rh) [17,29–33] to design and prepare ordered intermetallic nanocatalysts [34–39], high-entropy alloy [31] or core/shell [40–42] nanostructures, as the activity of Pt-based alloy catalysts can be further enhanced by synergistic interactions between different active components [39]. For geometric morphology control, 1D NWs possess large length/diameter (L/D) ratio and high surface atom exposure, which not only provide a large number of catalytic sites for electrocatalytic reactions, but also effectively prevent the aggregation during the electrocatalysis [43]. In addition, the 1D material provides an axial direction for the transfer of electrons and mass, which can provide excellent electrical conductivity for ORR electrocatalysts [43,44]. Interestingly, the non-noble metal

* Corresponding authors.
E-mail addresses: yipinghu@uestc.edu.cn (Y. Hu), qinyue@uestc.edu.cn (Q. Yue).

https://doi.org/10.1016/j.cclet.2023.108445
1001-8417/

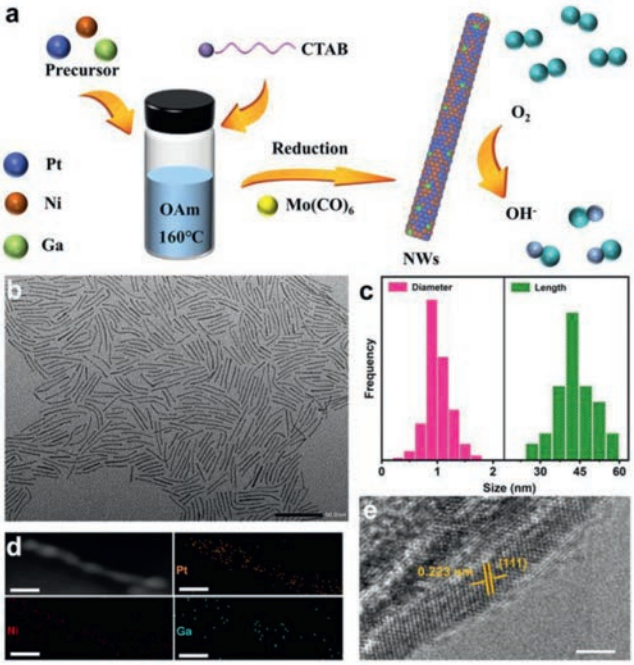

Fig. 1. (a) Scheme of the fabrication process for PtNiGa NWs and the catalysis mechanism in the oxygen reduction reaction. Structural and compositional characterizations of PtNiGa NWs: (b) TEM images. (c) Histogram of diameter and length distributions. (d) EDS elemental mapping images of Pt, Ni and Ga. (e) HRTEM images. Scale bars: (b) 50 nm, (d) 5 nm, (e) 2 nm.

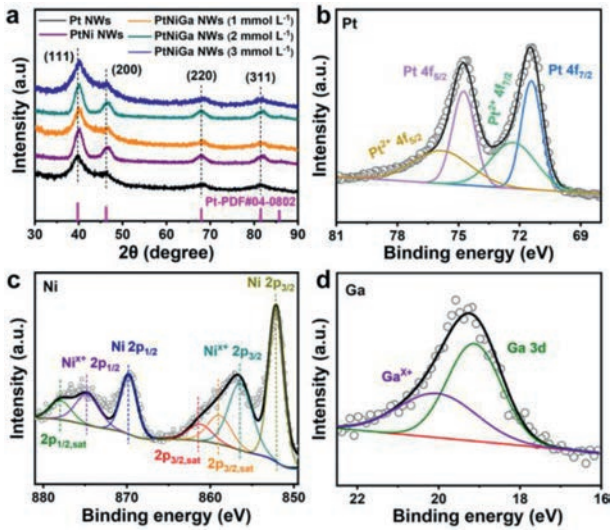

Fig. 2. (a) XRD patterns of Pt NWs/C, PtNi NWs/C and PtNiGa NWs/C. XPS spectra of (b) Pt 4f, (c) Ni 2p and (d) Ga 3d of PtNiGa NWs/C.

gallium (Ga) can be introduced into the Pt-based alloys to improve the durability of ORR owing to the Ga-induced stabilization of the octahedral structure by suppressing Pt migration and maintaining octahedral morphology [30]. Despite some progress made in the design of Pt-based alloy electrocatalysts for ORR, it still remains a great challenge to design and synthesize high-quality low-Pt alloys with special nanostructures (*e.g.*, 1D NWs) to achieve high activity and excellent durability for electrocatalyzing ORR.

In this study, an ultrathin ternary PtNiGa nanowire (PtNiGa NW) with one-dimensional geometry was synthesized by a simple wet chemical method for the simultaneous introduction of Ni and Ga (Fig. 1a). A third metal Ga having strong interaction with platinum is incorporated to bimetallic PtNi alloy nanocatalyst. The ternary PtNiGa NWs exhibit 11.2 times higher mass activity and 7.6 times higher specific activity than those of commercial Pt/C catalysts. The ultrafine nanowire structure and incorporating of small amounts of Ga atoms contribute the PtNiGa catalyst with extraordinary durability with a negligible activity decay over 10,000 cycles. The effective formation of ultrafine ternary PtNiGa NWs with distinct morphology and composition provides a significant approach to study the presence of a small amount of Ga atoms, structural effects, and alloy effect on ORR.

The structural characterizations and performance tests of the PtNiGa NWs prepared with a $Ga(acac)_3$ feeding amount of 2 mmol/L was carried out. Transmission electron microscope (TEM) image clearly shows that as-synthesized catalysts possess high-quality ultrathin nanowire structure (Fig. 1b) with an average diameter of 1.0 ± 0.5 nm and a length of 44 ± 12 nm (Fig. 1c) and the yield is nearly 100%. Furthermore, scanning transmission electron microscopy-energy dispersive spectroscopy (STEM-EDS) elemental mapping of the samples depicts the homogeneous distribution of Pt (orange), Ni (red), and Ga (blue) throughout the nanowire as shown in Fig. 1d and Fig. S1 (Supporting information). High-resolution TEM (HRTEM) image of the PtNiGa NWs also reveals highly crystallinity with a preferred face of (111) orientation with a clear interplanar spacing of 0.223 nm (Fig. 1e), which is similar with that of the PtNi NWs (0.225 nm) and smaller than of Pt NWs (0.23 nm), suggesting a slight compressive strain may exist (Fig. S2 in Supporting information). The powder X-ray diffraction (XRD) patterns (Fig. 2a) show that the peaks of Pt NWs, PtNi NWs and PtNiGa NWs with different amount of Ga well match with the standard PDF card of Pt (PDF#04–0802), demonstrating that heteroatomic Ga and Ni does not significantly change the alloy structure. All these samples are cubic crystal systems with a space group of Fm-3 m and show FCC phase. The XRD peak broadening is caused by the small grain size of the ultrafine nanowire. As shown in Fig. 2a, the diffraction peaks of PtNi NW show a slight positive shift compared to that of Pt NWs, which is due to the smaller radius of Ni atom than Pt atom. The XRD diffraction peaks of PtNiGa NWs almost overlap with those of PtNi NWs, mainly because the Ga atoms and Pt atoms have similar atomic radii, and the trace amount of Ga atoms introduced, in accordance with the varies of lattice space from the HRTEM results. Both the XRD and HRTEM results indicate that the transition metals Ni and Ga can induce a compressive strain. The elemental composition and the weight loading on the carbon support Vulcan XC-72 carbon of PtNiGa/C NWs before and after acid treatment were further determined using inductively coupled plasma optical emission spectroscopy (ICP-OES). The overall atomic ratio for Pt/Ni/Ga of the NWs was quantitatively determined as 71.1:23.0:5.6.

X-ray photoelectron spectroscopy (XPS) was employed to investigate the element state of PtNiGa NWs (Figs. 2b and c), and the high-resolution XPS spectrum of Pt 4f, Ni 2p and Ga 5d peaks are analyzed in detail. The high-resolution of Pt 4f is presented in Fig. 2b, which displays two doublets. The first doublet (71.85 eV) can be assigned to Pt $4f_{7/2}$, and the other one (75.12 eV) is fitted into Pt $4f_{5/2}$ [11]. The maximum peaks can be assigned to Pt^0 and weak peaks can attribute to Pt^{2+}, which indicates that Pt mainly presents the zero-valent. Similarly, the Ni also has two doublets, $2p_{3/2}$ and $2p_{1/2}$ (Fig. 2c) [45]. There are two spin orbit doublets, the first doublet at 853.02 eV and 869.24 eV and the second doublet at 856.3 eV and 874.6 eV is assigned to Ni^0 and Ni^{x+}, respectively. Ni^0 is also the main valence state presented [11]. Ga as a dopant whose binding energy is located at 20.4 eV can be attributed to Ga^{X+}, another peak (18.8 eV) is Ga^0 (Fig. 2d). Overall, Pt, Ni, and Ga appear predominantly in the zero-valent state, *i.e.*, Pt^0, Ni^0 and Ga^0. Some of the positive valence is due to the unavoid-

able slight surface oxidation when exposed to air. As a comparison catalyst, the high-resolution XPS of Pt and Ni in PtNi NWs has nearly the same binding energy as PtNiGa NWs, which indicates that the presence of Ga does not affect the formation of PtNi alloys (Fig. S3 in Supporting information). It is noted that the oxidation states content of Pt and Ni in the bimetallic PtNi MWs is significantly higher than PtNiGa NWs, especially for Ni, which again demonstrates that the presence of Ga can effectively suppress the oxidation of Pt and Ni, thus further enhancing the stability of catalysts.

To understand the growth mechanism of PtNiGa NWs, we carried out time-following experiments and implemented TEM-characterizations for these formed intermediate products. As shown in Fig. S4a (Supporting information), the product collected at the initial stage (5 min) is dominated by short nanorods. Upon increasing the reaction time (30 min), the nanorods grow into NWs (Fig. S4b in Supporting information). When the reaction process proceeds to 2 h, high-quality and 1.0 nm thick NWs were formed (Fig. S4c in Supporting information). The morphology and length remain constant with increasing reaction time (Fig. S4d in Supporting information). The time-dependent reaction mechanism explanation henceforth indicates the preferred anisotropic growth of nanocrystals to form the NWs. XRD patterns of ternary PtNiGa NWs obtained at different reaction times show that the reaction time does not significantly affect the formation of the alloy structure (Fig. S5 in Supporting information). We further studied the effect of different experimental parameters to control the morphology of the resultant PtNiGa alloys (Fig. S6 in Supporting information). Figs. S6a and b show no obvious nanowire morphology, indicating that the ratio of $Mo(Co)_6$ and CTAB significantly affects the formation of ternary PtNiGa NWs. Notably, the length of PtNiGa NWs can be easily controlled by changing the amounts of $Mo(CO)_6$ while other synthesis parameters such as, amount of (glucose, precursors and CTAB) and temperature remained constant (Figs. S6c and d). Using the same synthetic method in the absence of CTAB yielded heavily aggregated particles, whereas in the absence of glucose mixed morphologies of nanoparticles and short length nanowires were also formed respectively while other synthesis parameters remain unchanged (Figs. S6f and e). The influence of the feeding amount of $Ga(acac)_3$ precursor on the nanowire morphology was also investigated (Fig. S7 in Supporting information). Uniform nanowires with high quality can be obtained when the concentration of $Ga(acac)_3$ is between 1 mmol/L and 3 mmol/L (Figs. S7a-c). As the concentration of $Ga(acac)_3$ is increased to 5 mmol/L, the coexistence of nanoparticles and nanowires are observed and the nanowires become shorter (Fig. S7d).

For comparison, bimetallic PtNi NWs (Fig. S8a in Supporting information) and Pt NWs (Fig. S9a in Supporting information) are also prepared with the same synthetic procedure without introducing $Ga(acac)_3$ or/and $Ni(acac)_2$ precursor. Furthermore, the morphological and structural analysis demonstrated the formation of PtNi NWs with an average diameter of 1.0 ± 0.4 nm and a length of 45 ± 20 nm (Fig. S8b in Supporting information), while the average diameter of Pt NWs was 1.4 ± 0.4 nm and the length were 43 ± 15 nm (Fig. S9b in Supporting information). The nanowire lengths and diameters of pure Pt NWs, binary PtNi NWs, and ternary PtNiGa NWs do not differ significantly, therefore, the synthesis method is potentially universal for alloy nanowires.

Prior to ORR performance measurements, samples of PtNiGa NWs were deposited onto Vulcan XC-72 carbon and subsequently treated with acetic acid to remove residual surfactants, and their performance were compared with bimetallic PtNi NWs, Pt NWs and commercial Pt/C catalysts. The electrochemical active surface area (ECSA) of each catalyst were determined from the charge obtained using underpotentially deposited hydrogen adsorption region after double-layer correction and assuming a value

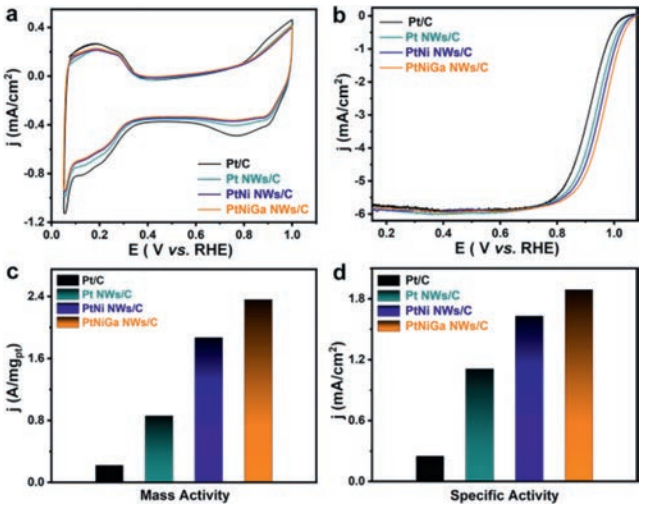

Fig. 3. Electrocatalytic performance of different catalysts. (a) Cyclic voltammograms of recorded in Ar-saturated 0.1 mol/L $HClO_4$ solution with a scan rate of 50 mV/s at room temperature. (b) Positive-going polarization curves recorded in O_2-saturated 0.1 mol/L $HClO_4$ solutions with a sweep rate of 20 mV/s and a rotation rate of 1600 rpm. (c) Mass activities at 0.9 V *vs.* RHE. (d) Specific activities at 0.9 V *vs.* RHE for Pt/C, Pt NWs/C, PtNi NWs/C and PtNiGa NWs/C.

of 210 μC/cm^2 for the adsorption of a hydrogen monolayer (Fig. 3a). The ECSA of PtNiGa NWs/C of 96.23 m^2/g_{Pt} revealed much larger than those of bimetallic PtNi NWs/C catalyst (86.9 m^2/g_{Pt}), Pt NWs/C catalyst (74. 57 m^2/g_{Pt}) and commercial Pt/C catalyst (64.17m^2/g_{Pt}). Fig. 3b shows the positive-going ORR polarization curves of the catalysts conducted in O_2-saturated 0.1 mol/L $HClO_4$ solution at a sweep rate of 20 mV/s using the rotating disk electrode (RDE) method at room temperature, and the ternary PtNiGa NWs exhibits the best ORR activity. The study of the ORR activity of the ternary PtNiGa NWs prepared with different $Ga(acac)_3$ precursor addition amounts showed that the best activity was achieved when the $Ga(acac)_3$ addition amount was 0.010 mmol (Fig. S10a in Supporting information). To evaluate the surface effects and mass of all catalysts, the kinetic current was determined based on the Koutecky-Levich equation and then normalized against the ECSA and Pt mass loading to determine the mass and specific activity, respectively (Figs. 3c and d). The results for PtNiGa NWs reveal the highest mass activity of 2.37 A/mg_{Pt} compared to bimetallic PtNi NWs (1.85A/mg_{Pt}), Pt NWs (1.17 A/mg_{Pt}) and commercial Pt/C (0.21 A/mg_{Pt}) catalysts. The specific activity of PtNiGa NWs (1.89 mA/cm^2) shows also better enhancement, over bimetallic PtNi NWs (1.64 mA/cm^2), Pt NWs (0.87 mA/cm^2), and commercial Pt/C (0.25 mA/cm^2) catalysts. Electrochemical Impedance Spectroscopy (EIS) studies show that the prepared PtNiGa NWs has the lowest resistance compared with PtNi NWs and Pt NWs (Fig. S10b in Supporting information), indicating that the incorporation of the 3d transition metal Ga optimizes the electronic state of the ternary PtNiGa NWs and facilitates the electron transport during the ORR process. The as-synthesized PtNiGa NWs catalyst demonstrated higher ORR performance capability over bimetallic PtNi nanowires thereby signifying that Ga atoms had positively contributed to the surface activity of the catalyst.

In addition to activity, the long-term durability of catalyst is also a critical parameter for ORR. As shown in Fig. 4a. After 10,000 cycles PtNiGa NWs shows excellent durability with largely retained its activity, showing no loss for its half-wave potential and still shows high mass activity (2.08 A/mg). Besides, we examine the changes of ECSA, specific and mass activity for PtNiGa NWs/C, PtNi NWs/C, Pt NWs/C, and commercial Pt/C catalysts by comparing to

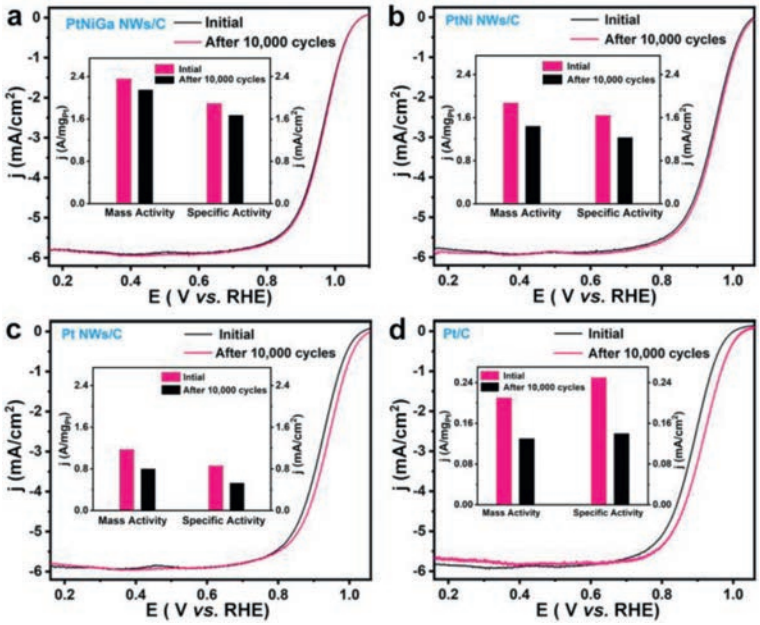

Fig. 4. Electrochemical durability of catalysts. (a) ORR polarization curves and the corresponding mass and specific activities (insert) of PtNiGa NWs/C. (b) ORR polarization curves and the corresponding mass and specific activities (insert) of PtNi NWs/C. (c) ORR polarization curves and the corresponding mass and specific activities (insert) of Pt NWs/C. (d) ORR polarization curves and the corresponding mass and specific activities (insert) of commercial Pt/C measured before and after 10,000 cycles.

their initial ECSA, specific and mass activity measured at 0.9 V *vs.* RHE (Figs. 4b-d). PtNiGa NWs/C exhibits less ORR activity loss, about 11.6% in a specific activity, 12.8% in mass activity, and by contrast, the commercial Pt/C loss as large as 44.21% in specific activity and mass activity 38.1%, respectively (Fig. 4d). Interestingly, PtNiGa NWs/C catalysts show a very small percentage decrease in their initial ECSA (6%), while PtNi NWs/C showed a large decrease of ECSA (31%) after 10,000 cycles. By contrast, the commercial Pt/C shows the biggest loss of ECSA (37%). The stability of the geometric morphology also indicates that the alloy catalysts are not prone to dissolution and reconstitution. By comparing the TEM images before and after testing of different catalysts, it can be found that PtNiGa NWs maintain the nanowire morphology better than PtNi NWs (Fig. S11 in Supporting information), while both Pt NWs and commercial Pt/C undergo more severe agglomeration, especially for the commercial Pt/C (Fig. S11). This further indicates that Ga is beneficial for stabilizing the geometry of the ternary alloy PtNiGa NWs.

The compositional analysis after 10,000 cycles conducted by ICP-OES suggested that the Pt/Ni/Ga atomic ratio changed from 71.1:23.0:5.6 to 73.5:20.2:6.3, slightly changing from the initial atomic ratio, with a very slight decrease in Ni content. By contrast, the atomic ratio of Pt/Ni for bimetallic PtNi NWs catalyst changed from 2.99:1.00 to 12.32:1.00, as previous reported [11]. The large change in composition for the bimetallic PtNi NWs catalyst is supposed to rise the damage of its microstructure, causing its lower catalytic durability. It is concluding the introduction of Ga does effectively inhibit Ni dissolution. Most importantly, the excellent durability of PtNiGa/C NWs catalyst most likely arises from (1) their ultrafine nanowires structure which can suppress the ripening process and reinforce the contact between NW catalyst with the carbon support [11,28]; and (2) the incorporation of the 3d transition metals Ga, which helps to stabilize the electronic states of the Pt-based alloy catalysts and reduce the dissolution of Ni and inhibit the oxidation state of Pt and Ni, thus enhancing the structural stability of the ORR catalysts. The doping of Ga reduces the exophilic of the PtNi surface while the resulting compressive strain enhances the durability of the catalyst [28,30,46]. Table S1 (Supporting information) summaries the activity/durability comparation of the reported Pt-based electrocatalysts and the PtNiGa/C NWs, revealing that the ternary PtNiGa NWs exhibited overall superior performance among these Pt-based catalysts.

In summary, we have demonstrated a synthetic strategy to successfully prepare PtNiGa/C NWs catalysts with high-quality ultrafine nanowires with diameter of 1.0 ± 0.5 nm which exhibits high activity and durability for ORR. PtNiGa/C NWs catalyst with ultrafine diameter exhibits superior activity with 11.2- and 7.6-times fold enhancement on mass activity and specific activity than commercial Pt/C, respectively. The enhanced catalytic durability originated from the ultrafine diameter 1D nanostructure, and incorporated a small amount of Ga atoms, making it a superior durable catalyst towards ORR. Furthermore, the mass activity of PtNiGa/C NWs catalyst decreased only by 12.8% and largely retain its ECSA after 10000 potential cycles, comparing to 38% for commercial Pt/C catalyst. Therefore, this work effectively improves the ORR activity and stability of Pt-based catalysts through the reasonable introduction of Ga heteroatoms and the combination of 1D geometry. This study not only achieves a highly active and robust ORR catalyst but also demonstrates a general guidance for the rational design and synthesis of the ternary Pt-based nanowire catalysts for outstanding ORR performance.

Declaration of competing interest

The authors declare that they have no known competing financial interests or personal relationships that could have appeared to influence the work reported in this paper.

Acknowledgments

This work was supported by the National Youth Top-notch Talent Support Program of China, and the Sichuan Science and Technology Program (No. 2020YJ0243), Foundation of State Key Laboratory of High-efficiency Utilization of Coal and Green Chemical Engineering (No. 2022-K28).

Supplementary materials

Supplementary material associated with this article can be found, in the online version, at doi:10.1016/j.cclet.2023.108445.

References

[1] D. Feng, Y. Dong, P. Nie, L. Zhang, Z.A. Qiao, Chem. Eng. J. 430 (2022) 132883.
[2] Y. Song, Y. Peng, S. Yao, et al., Chin. Chem. Lett. 33 (2022) 1047–1050.
[3] F. Guo, M. Zhang, S. Yi, et al., Nano Res. Energy 1 (2022) 9120027.
[4] H. Jin, S. Zou, Q. Wen, et al., Chin. Chem. Lett. 34 (2023) 107441.
[5] K. Wang, N. Li, Y. Yang, et al., Chin. Chem. Lett. 32 (2021) 3159–3163.
[6] L. Zhao, J. Zhu, Y. Zheng, et al., Adv. Energy Mater. 12 (2022) 2102665.
[7] H. Xu, H. Shang, C. Wang, Y. Du, Adv. Funct. Mater. 30 (2020) 2006317.
[8] R. Chen, T. Shu, F. Zhao, et al., Nano Res. 15 (2022) 9010–9018.
[9] C. Chen, Y. Kang, Z. Huo, et al., Science 343 (2014) 1339–1343.
[10] S.M. Dull, O. Vinogradova, et al., ACS Appl. Energy Mater. 5 (2022) 8282–8291.
[11] K. Li, X. Li, H. Huang, et al., J. Am. Chem. Soc. 140 (2018) 16159–16167.
[12] G. Nie, Z. Zhang, T. Wang, C. Wang, Z. Kou, ACS Appl. Mater. Interfaces 13 (2021) 37961–37978.
[13] L. Chong, J. Wen, J. Kubal, et al., Science 362 (2018) 1276–1281.
[14] V.R. Stamenkovic, B.S. Mun, M. Arenz, et al., Nat. Mater. 6 (2007) 241–247.
[15] T.H. Yang, J. Ahn, S. Shi, et al., Chem. Rev. 121 (2021) 796–833.
[16] Z. Yang, L. Shang, X. Xiong, et al., Chem. Eur. J. 26 (2020) 4090–4096.
[17] X. Huang, Z. Zhao, L. Cao, et al., Science 348 (2015) 1230–1234.
[18] M. Escudero-Escribano, P. Malacrida, M.H. Hansen, et al., Science 352 (2016) 73–76.
[19] X. Wang, L. Figueroa-Cosme, X. Yang, et al., Nano Lett. 16 (2016) 1467–1471.
[20] F. Kong, Z. Ren, M.N. Banis, et al., ACS Catal. 10 (2020) 4205–4214.
[21] M. Li, F. Tian, T. Lin, et al., Small Methods 5 (2021) 2100154.
[22] C. Wang, M. Chi, D. Li, et al., J. Am. Chem. Soc. 133 (2011) 14396–14403.
[23] H. Huang, K. Li, Z. Chen, et al., J. Am. Chem. Soc. 139 (2017) 8152–8159.
[24] H. Zhu, S. Zhang, S. Guo, D. Su, S. Sun, J. Am. Chem. Soc. 135 (2013) 7130–7133.
[25] W. Zhang, Y. Yang, B. Huang, F. Lv, et al., Adv. Mater. 31 (2019) 1805833.
[26] Z. Yao, Y. Yuan, T. Cheng, et al., Nano Lett. 21 (2021) 9354–9360.
[27] L. Sahoo, R. Garg, K. Kaur, C.P. Vinod, U.K. Gautam, Nano Lett. 22 (2022) 246–254.
[28] L. Gao, X. Li, Z. Yao, et al., J. Am. Chem. Soc. 141 (2019) 18083–18090.
[29] Y. Li, F. Quan, L. Chen, et al., RSC Adv. 4 (2014) 1895–1899.
[30] J. Lim, H. Shin, M. Kim, et al., Nano Lett. 18 (2018) 2450–2458.
[31] Y. Yu, F. Xia, C. Wang, et al., Nano Res. 15 (2022) 7868–7876.
[32] R. Shen, X. Wu, X. Li, et al., ChemistrySelect 6 (2021) 3891–3896.
[33] A. Zhang, Y. Liang, H. Zhang, Z. Geng, J. Zeng, Chem. Soc. Rev. 50 (2021) 9817–9844.
[34] X.X. Wang, S. Hwang, Y.T. Pan, et al., Nano Lett. 18 (2018) 4163–4171.
[35] Y. Yan, J.S. Du, K.D. Gilroy, et al., Adv. Mater. 29 (2017) 1605997.
[36] V.B. Kumar, J. Sanetuntikul, P. Ganesan, et al., Electrochim. Acta 190 (2016) 659–667.
[37] J. Lim, C. Jung, D. Hong, et al., J. Mater. Chem. A 10 (2022) 7399–7408.
[38] H.Y. Kim, T. Kwon, Y. Ha, et al., Nano Lett. 20 (2020) 7413–7421.
[39] H. Ma, Z. Zheng, H. Zhao, et al., J. Mater. Chem. A 9 (2021) 23444–23450.
[40] P. Weber, D.J. Weber, C. Dosche, M. Oezaslan, ACS Catal. 12 (2022) 6394–6408.
[41] D. Liu, N. Yang, Q. Zeng, et al., Chin. Chem. Lett. 32 (2021) 3288–3297.
[42] J. Guan, S. Yang, T. Liu, et al., Angew. Chem. Int. Ed. 60 (2021) 21899–21904.
[43] Q. Shao, K. Lu, X. Huang, Small Methods 3 (2019) 1800545.
[44] Z. Yang, H. Yang, L. Shang, T. Zhang, Angew. Chem. Int. Ed. 61 (2022) e202113278.
[45] B. Fang, X. Chu, X. Han, et al., Chem. Commun. 58 (2022) 13803–13806.
[46] D.A. Torelli, S.A. Francis, J.C. Crompton, et al., ACS Catal. 6 (2016) 2100–2104.